Science Bulletin 64 (2019) 1158–1166

Contents lists available at ScienceDirect

Science Bulletin

journal homepage: www.elsevier.com/locate/scib

Science Bulletin
www.scibull.com

Article

Axial ligands tailoring the ORR activity of cobalt porphyrin

Yue Zhou, Yong-Fang Xing, Jing Wen, Hai-Bo Ma *, Feng-Bin Wang *, Xing-Hua Xia *

School of Chemistry and Chemical Engineering, Nanjing University, Nanjing 210023, China

ARTICLE INFO

Article history:
Received 24 April 2019
Received in revised form 18 June 2019
Accepted 26 June 2019
Available online 2 July 2019

Keywords:
Oxygen reduction reaction (ORR)
Cobalt porphyrin
Axial ligands
Push effect

ABSTRACT

In an effort to provide visualization and understanding to the electronic "push effect" of axial ligands on the catalytic activity of cobalt macrocyclic molecules, we design a simple model system involving an [5,10,15,20-tetrakis(4-methoxyphenyl)porphyrin]cobalt(II) (TMMPCo) monolayer axially-coordinated on thiol ligand modified Au electrode and explore the activity of the axial-ligand coordinated TMPPCo toward oxygen reduction reaction (ORR) in acidic medium. Three different ligands, with a decreasing order of coordinating ability as: 4-mercaptopyridine (MPy) > 4-aminothiolphenol (APT) > 4-mercaptobenzonitrile (MBN) are used and a maximum difference in ORR onset potential of 80 mV is observed between the MPy (highest onset potential) and MBN systems (lowest onset potential). The ORR activity of TMPPCo increases with the increase in binding strength of the axial ligand. A detailed mechanism study reveals that ORR on the three ligand coordinated TMPPCo systems shares the same 2-electron mechanism with H_2O_2 as the terminal product. Theoretical calculation into the structure of the ligand coordinated cobalt porphyrins uncovers the variation in atomic charge of the Co(II) center and altered frontier molecular orbital distribution among the three ligand systems. Both properties have great influence on the back-bonding formation between the Co(II) center and O_2 molecules, which has been suggested to be critical toward the O_2 adsorption and subsequent activation process.

© 2019 Science China Press. Published by Elsevier B.V. and Science China Press. All rights reserved.

1. Introduction

The transition metal-based N_4-metallomacrocyclic molecules, especially transitional metal (TM) based metalloporphyrins, metallophthalocyanines and more recently the metallocorroles serve as a promising alternative family for ORR catalysts ever since their electrocatalytic activity was first uncovered in 1964 [1–8]. The superiority of these materials is their much lower cost compared to noble metal Pt based catalysts [9], and their high CO tolerance [10,11]. Another attractive feature for these molecules is their easily tailored catalytic activity. The active center for N_4-metallomacrocyclic materials is easy to be defined, and their activity could be tuned through the substitution on the central metal ion [12,13], or the modifications on the structure of the N_4-macrocyclic ligand [14,15].

The naturally existing metalloporphyrins take part in various important biological processes and their activities have been found to be related to their axial ligands [16–22]. Inspired by this point, numerous biomimetic materials with brilliant catalytic performance have been prepared. A molecular assembly of Cu(3,3′-diaminobenzidine) polymeric complex on carbon black has been reported with high hydrazine oxidation reaction (HOR) and ORR activity, in which the 3,3′-diaminobenzidine ligand functions like the Cys-His group in natural laccases in fine tuning the electronic structure of the Cu center [23]. Cao and co-workers [21] reported on a highly efficient ORR catalyst (SWCNT-Py-PcFe) and the presence of a pyridine ligand in the axial vacancy of PcFe has been highlighted. The role of axial ligand on metallomacrocyclic molecules has been interpreted as being through the "push effect". Namely, the axial coordination of ligand group on the central metal increases the electron density on the macrocycle ring through donating electrons toward the unoccupied *d*-orbitals of the metal ion, and therefore affects its catalytic activity. Detailed studies concerning the role of axial ligands on the activity of metallomacrocycles have been conducted to address the "push effect" [24–26]. However, these studies mainly focuses on the Fe porphyrins since the "push effect" is mostly pronounced in Fe porphyrin-based active centers in natural systems [27–29]. In contrast, few attentions have been paid to other metal based macrocycles, such as cobalt porphyrins, which is another popular family of promising electrocatalysts. Unlike Fe ion, Co is not involved in the Fenton reaction, which could cause damage to the carbon skeleton of material and also lead to the demetallation of the central ion. Therefore, the Co macrocycle catalyst usually exhibits a better

* Corresponding authors.
E-mail addresses: haibo@nju.edu.cn (H.-B. Ma), fbwang@nju.edu.cn (F.-B. Wang), xhxia@nju.edu.cn (X.-H. Xia).

https://doi.org/10.1016/j.scib.2019.07.003
2095-9273/© 2019 Science China Press. Published by Elsevier B.V. and Science China Press. All rights reserved.

long-term stability especially in acidic medium compared with the Fe family [30]. Therefore, from the aspect of tailoring the ORR activity of the central Co ion through more efficient means, the function of its axial ligand deserves to be systematically studied.

In this study, a model system built on Au electrode has been designed to study the effect of axial ligands on the ORR activity of cobalt N_4-macrocycles. [5,10,15,20-tetrakis(4-methoxyphenyl) porphyrin]cobalt(II) (TMPPCo) is chosen as the molecule and three aromatic thiol ligands: 4-mercaptopyridine (MPy), 4-aminothiolphenol (APT) and 4-mercaptobenzonitrile (MBN) are used as the axial ligands. These thiol ligands could spontaneously form self-assembled monolayer (with ligating header groups) on Au electrode surface through the formation of Au-S covalent bond and TMPPCo could be assembled on the surface through the axial coordination interaction between its central cobalt ion and the ligand header groups of SAM. The difference for the three ligand coordinated TMPPCo systems in catalytic activity toward ORR in acidic medium has been investigated together with detailed mechanism study using RDE and RRDE techniques. Combined with the computational results, a deeper understanding toward the "push effect" of axial ligand for cobalt porphyrins has been realized.

2. Experimental

2.1. Reagents

TMPPCo (≥96%) was purchased from TCI (China). MPy (95%), APT (97%) were obtained from Sigma (USA). MBN (95%) was purchased from Nanjing Norris Pharm Technology Co. Ltd (China). Methyl 4-aminobenzoate (≥98%), 4-cyanobenzoic acid methyl ester (≥98%) methyl isonicotinate (≥98%) and methyl benzoate (≥99%) were from Admas-beta (China). Aqueous solutions were prepared using ultrapure water with resistance above 18.2 MΩ cm (Millipore, USA).

UV–vis absorption spectra of TMPPCo solutions were obtained on a UV-1800 spectrometer (Shimadzu, Japan). The surface-enhanced Raman scattering (SERS) spectra for the ligand modified Au substrates were collected in air under a Renishaw laser confocal Raman microscope (Renishaw, UK), using a 633 nm laser beam as the light source.

2.2. Electrochemical measurements

Electrochemical measurements were carried out on a CHI 660E (CHI, USA) electrochemical workstation using a conventional three-electrode configuration. The gold electrode (2 mm in diameter, CHI) was used as the working electrode (WE), a Pt wire was employed as the counter electrode (CE) and the reference electrode (RE) was an Ag/AgCl electrode (backfilled with saturated KCl solution, Gaoss Union, Wuhan). The potential is converted to be versus reversible hydrogen electrode (RHE) using the equation: $E_{vs.RHE} = E_{vs.Ag/AgCl} + 0.197 + 0.0591 \times pH$. Before use, the gold disk electrode was polished in aqueous slurries containing 0.05 μm alumina oxide powders and sonicated in ethanol and deionized water successively.

The rotating disk electrode (RDE) and rotating ring-disk electrode (RRDE) tests were carried out using a rotating electrode setup (PINE Research, USA) with an MSR rotator shaft. The RDE experiment was carried out using an AFE7R8 ring-disk electrode from PINE Research. The RRDE electrode was an AFE6R1 Change Disk ring-disk electrode from PINE Research including a polytetrafluoroethylene (PTFE) body tip, an Au disk insert (5 mm in diameter) and a Pt ring (1 mm in width). The officially provided collection efficiency (N) for this RRDE setup is 25.6% and was experimentally confirmed prior to use (Fig. S1 online).

2.3. Two-step modification for TMPPCo-ligand modified Au disk electrode

An Au electrode was first pretreated using the procedure as described above. Before modification, the electrode was electrochemically cycled between −0.3 and 1.5 V in 0.5 mol/L H_2SO_4 for 100 cycles at a scan rate of 100 mV/s to gain a better activity. After it was washed with deionized water and dried under N_2 stream, this freshly activated electrode was immersed into an ethanol solution containing 1 mmol/L thiol ligand to attach the SAM molecules onto the electrode surface through the formation of Au-S covalent bond. After incubating at 4 °C for 12 h, the electrode was taken out and rinsed thoroughly with pure ethanol thrice followed by drying under N_2 stream. This ligand modified Au electrode was then immersed into CH_2Cl_2 solution containing 1 mmol/L TMPPCo to assemble the cobalt porphyrin onto the surface through the axial coordination reaction between the porphyrin Co(II) center and the ligating header group of the thiol ligand pre-assembled on Au surface. The reaction was allowed to proceed at 4 °C for 4 h in dark. The two-step modified Au electrode was then taken out and washed with pure CH_2Cl_2 to remove the weakly adsorbed TMPPCo and dried under N_2 stream. Fig. 1a depicts the schematic illustration on these two-step modification of the Au electrode.

2.4. Fabrication of SERS-active substrate

The Au electrode used for SERS measurements included a removable Au plate insert (2 mm in Au diameter) and a polyether ether ketone (PEEK) body tip which was purchased from Gaoss Union. To fabricate the SERS active substrate, this electrode was roughened using the electrochemical oxidation-reduction cycling (ORC) method [31]. The electrode was electrochemically polished in 0.5 mol/L H_2SO_4 to remove impurities and gain better activity. The freshly activated electrode was then cycled in 0.1 mol/L KCl between the potentials of Au oxide formation (1.2 V vs. sat. Ag/AgCl RE) and −0.5 V for 40 cycles at a scan rate of 50 mV/s. After completing the cycle, a bias equal to the reduction peak potential in the cyclic voltammogram was applied onto the electrode to ensure a complete reduction of the Au oxide. The gold plate was then demounted from the body and rinsed thoroughly with deionized water to remove the surface remaining chloride ions. The gold plate changed from bright yellow to dark brown with an obvious porous layer covered on its surface, indicating the successful roughening of the electrode. The porous structure of the roughened Au substrate was confirmed by scanning electron microscopy (SEM), which is obviously different from the planar morphology of the bare Au electrode (Fig. S2 online). This roughened gold plate was stored in deionized water at 4 °C before use. To measure the SERS spectrum of the assembled thiol ligands on Au, the plate was subjected to similar modifying procedure like that for the Au plate electrode.

2.5. Computational details

To further describe how the different axial ligands effect the electronic structures of cobalt porphyrin and successive activation process of adsorbate dioxygen, density functional theory (DFT) based geometry optimizations and frontier molecular orbital analyses were performed with the Gaussian 09 D.01 package [32]. The exchange-correlation energy for all the calculated complexes was described with the hybrid M06-2X density functional, with the TZVP basis set, which was used in our previous publication and also found to give relatively accurate geometric and electronic structures for metal-organic complexes [33]. To compromise the efficiency and accuracy of the computation, the four methoxyphenyl substituent groups on the *meso*-position of TMPPCo were replaced by Hydrogen atoms.

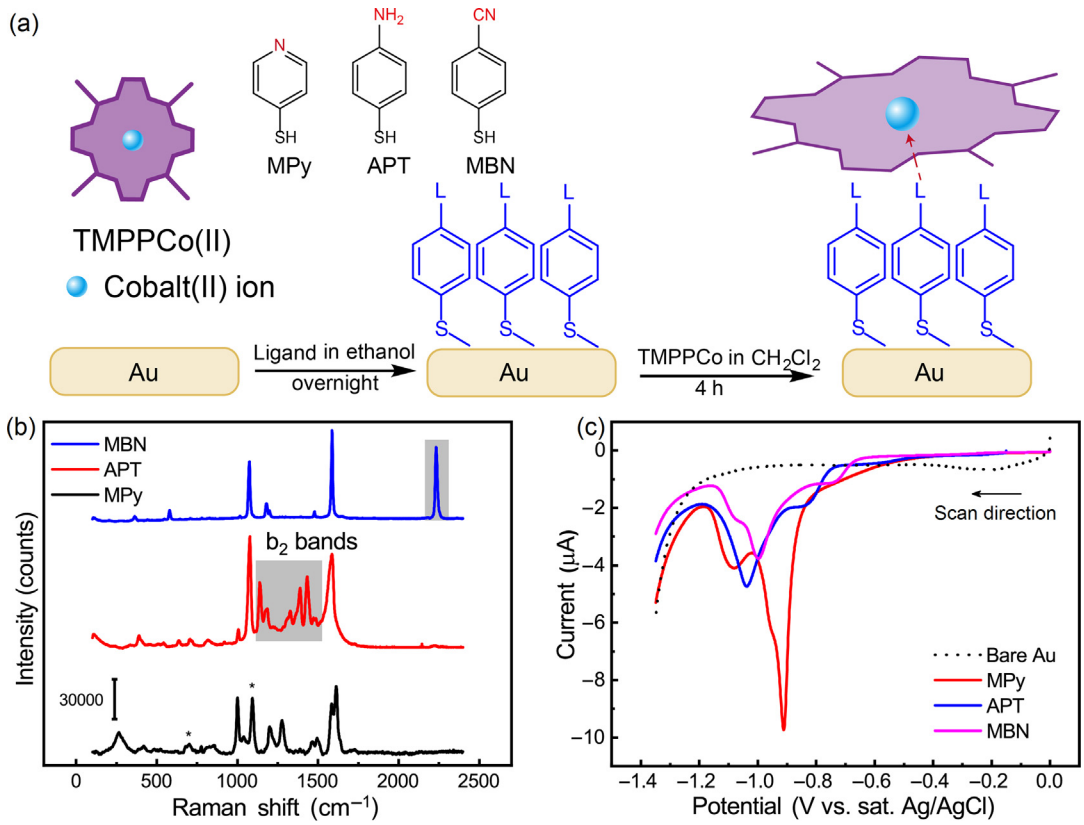

Fig. 1. (a) Schematic illustration on the two steps of modification on Au electrode. (b) SERS spectra collected on the ORC roughened SERS active Au substrate. (c) Reductive desorption LSVs of MPy, APT and MBN coated Au electrode in N_2 saturated 0.1 mol/L NaOH at a scan rate of 50 mV/s.

3. Results and discussion

3.1. SERS characterization on ligand SAMs

To confirm the assembly of thiol ligands on Au surface with a preferred orientation for later porphyrin axial coordination (exposing the ligating header group), SERS spectra of the three thiol ligands were collected on a roughened Au substrate fabricated by an electrochemical oxidation-reduction cycling (ORC) protocol. Fig. 1b presents the SERS spectra of the three thiol ligands. For MBN, its SERS spectrum (blue curve) is dominated by peaks attributable to the in plane vibration modes, which excludes the possibility that the molecule adsorbs in a flat conformation according to the surface selection rule in the electromagnetic enhancement theory for SERS [34], indicating that the benzene ring is at least titled in some angle to the substrate surface. The intense peak at 2,232 cm^{-1} belongs to the stretching mode of the —CN group [35]. This peak position is very close to that of neat state, which indicates that molecule adsorption with —CN group is unlikely, since the interaction of —CN with metal substrate would induce significant peak position shift of the —CN stretching mode [36]. In the SERS spectrum of APT molecule (red curve), the several intense b_2-type bands in the region between 1,100 and 1,500 cm^{-1} are the characteristics of the —NH_2 derivatives and provide direct evidence of APT adsorption on the surface with the —NH_2 ligand group unperturbed [37]. Once again, the enhancement of the several strong in-plane vibration bands denies the assumption that the APT might adsorb in a flat conformation [38]. Conversely, a titled or even vertical surface orientation is more rational. For MPy molecule (black curve), its adsorption mode on SERS active substrate could be analyzed by checking the band information of the so called X-sensitive bands relative to those of neat sample [39]. The two X-sensitive bands are marked with an asterisk (*) on the spectrum. The $6a_1$ band (β_{C-C}/ν_{C-S}) at 703 cm^{-1} has its counterpart in the spectrum of neat MPy sample at around 721 cm^{-1} and the $12a_1$ band ($\nu_{ring\ breathing}/\nu_{C-S}$) at 1,093 cm^{-1} is significantly enhanced compared with that of neat sample. The downshift of the $6a_1$ band and enhancement of the $12a_1$ band suggest that the adsorption of MPy might involve the participation of —SH group [40]. Although the SERS study does not provide direct spectral information for the Au—S bond, the SERS spectra of all the three ligands present adequate evidence for ligand adsorption on the gold substrate with a titled surface orientation while exposing the ligand groups outward, and probably the involvement of SH group during the adsorption process.

3.2. Reductive desorption of SAMs

Electro-reductive stripping-off protocol has been employed to confirm the formation of Au-S bond between the thiol ligand and Au surface [41]. The Au electrodes before and after the modification of ligand molecules were subjected to the linear scanning voltammetry (LSV) from the open circuit potential (OCP) to −1.35 V in N_2 saturated 0.1 mol/L NaOH and the results are shown in Fig. 1c. As is shown, starting at ca. −0.6 V, the desorption curves of all the thiol ligands show two to three reduction peaks at lower potentials, which could be ascribed to the reductive desorption process of thiol ligands with different adsorption strengths from the polycrystalline Au surface [42,43]. The calculated surface coverage density for MPy, APT, and MBN ligand thiols are 7.9×10^{-10}, 4.3×10^{-10} and 3.9×10^{-10} mol/cm^2, respectively. The slightly varied surface coverage densities for the three ligands might be due to their structural difference and different adsorption orientations on the surface [44]. The polarization curve of the bare

gold electrode does not show such reductive peaks at the same potential region, the small reduction peak at round −0.2 V could be due to the electrochemical reduction of the residual O_2 molecules adsorbed on the high active bare gold electrode surface. The reductive desorption result clearly demonstrates that these three thiol ligands have been successfully assembled on the Au surface via forming Au-S covalent bond.

3.3. ORR activity in acidic medium

The assembly of TMPPCo on the thiol ligand modified gold electrode is accomplished through the axial coordination reaction between its Co(II) center and the surface-exposing ligating groups. The feasibility for this assembling approach and a decreasing coordinating ability order for the used three ligands as MPy > APT > MBN has been confirmed by a solution phase UV–vis absorption spectroscopic study (Fig. S3 online). The ORR activity of the electrodes after TMPPCo assembly were examined for all the three ligand systems in acidic medium. In Fig. 2, the solid lines depict the cyclic voltammograms (CVs) for ORR, while the dashed lines represent the CVs measured under N_2 atmosphere. Faradaic peaks could not be distinguished in the CVs in N_2 saturated solution for all the three ligand-coordinated TMPPCo systems, giving rise to no direct electron transfer information between the porphyrin Co center and the electrodes. However, a good electrocatalytic activity toward substrate molecule requires efficient direct electron transfer between the electrode and the catalytic active center [22,45], which in this work is the Co(II) center of TMPPCo. The good catalytic activity toward O_2 electro-reduction undoubtedly demonstrates the facile electron transfer between the Co(II) ion and the electrode for all the three systems. The inability for measuring the redox signal of cobalt (II) ion could arise from that the redox potential of Co^{3+}/Co^{2+} and Co^{2+}/Co^{+} pair is beyond the potential regime of ORR, which means that the redox process of the Co(II) center is not involved in ORR. This finding has been reported by many studies concerning the cobalt porphyrin or phthalocyanine based catalysts for ORR [3,12,13,46]. Meanwhile, the ORR activity of ligand coated Au electrode without further assembly of TMPPCo has been measured, which demonstrates the excellent blocking capability of the ligand molecules toward the active Au surface (Fig. S4 online). Therefore, the Au electrode only functions as a conducting substrate which provides a steady electron flux toward the surface-attached TMPPCo catalyst and negligible contribution in the overall ORR current could come from the underlying Au active site. The difference in ORR activities among the three ligand systems is shown in Fig. 2d. Since the ORR current density given in our model system is relatively small, the onset potential has been defined as the potential at which ORR polarization curve deviates from the N_2 background. The CV of the MPy ligand shows an ORR onset potential at round 0.53 V. The ORR peak potential and peak current density are 0.3 V and 0.46 mA/cm^2, respectively. The catalytic curve of the APT ligand exhibits an ORR onset and peak potentials at 0.48 and 0.23 V, respectively, while the peak current density is 0.45 mA/cm^2. The curve of the MBN ligand presents an ORR onset and peak potential at 0.45 and 0.17 V respectively, while its peak current is 0.32 mA/cm^2. From the comparison on the onset potentials, a decreasing order in ORR activity for ligand coordinated TMPPCo could be derived in the ligand order as: MPy > APT > MBN, with MPy coordinated TMPPCo being the most efficient platform for ORR. The onset potential differs by 80 mV at most between the MPy and MBN systems. It should be noted that despite having different ORR onset potentials, the three ligand systems have the same curve shape in the mixed-controlled potential regime (inset), suggesting that the O_2 reduction reaction follows similar mechanism on the Co(II) center of TMPPCo, axially coordinated by three different ligands.

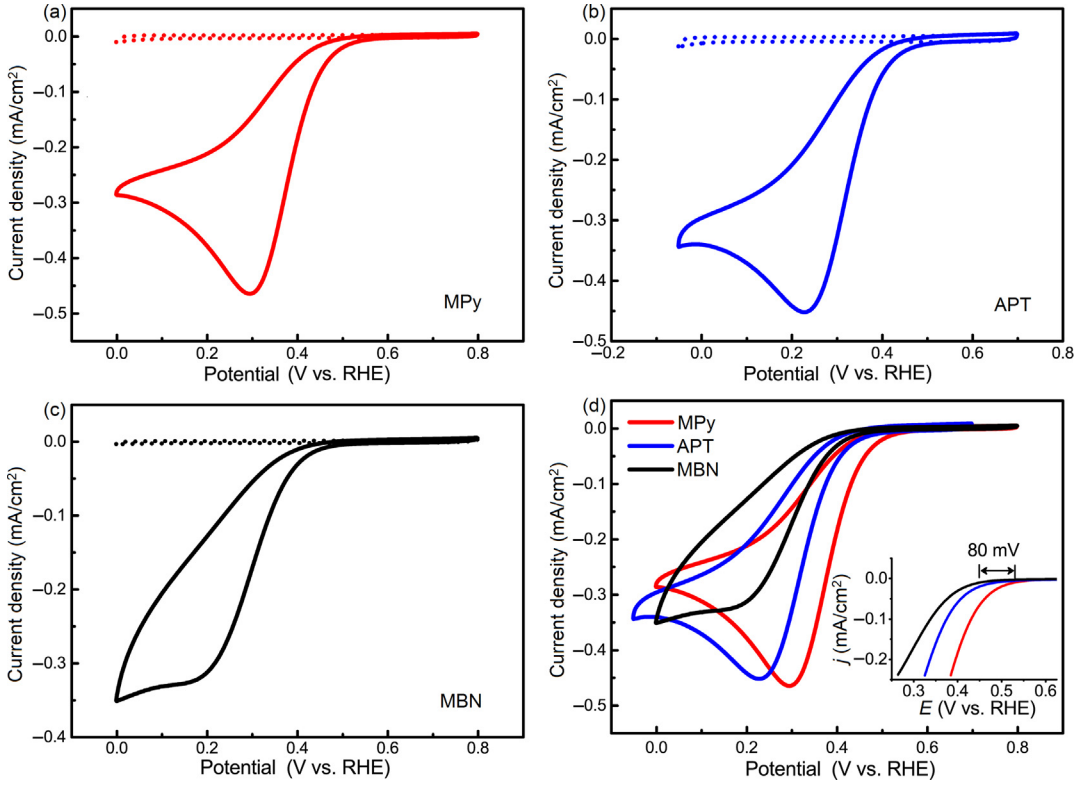

Fig. 2. (Color online) CVs of the gold electrodes modified with (a) MPy, (b) APT and (c) MBN coordinated TMPPCo in O_2 saturated 0.5 mol/L H_2SO_4 (solid lines) and CVs measured in N_2 saturated atmosphere at a scan rate of 50 mV/s (dashed lines). (d) A summary on the three ORR curves together with a comparison on the onset potentials (inset) in the low polarization regime.

3.4. ORR mechanism study

RDE technique has been used to study the ORR mechanism on three kinds of electrode surface. The ORR performance measured under hydrodynamic condition reproduces the activity order as observed without disk rotation, with MPy-TMPPCo having the highest onset potential while MBN-TMPPCo giving the lowest value (Fig. 3a, c and e). The as derived Koutecky-Levich plots which depict the relationship between $1/i$ and $\omega^{-1/2}$ under certain potentials are presented in Fig. 3 (right panels). The good linearity presented by the K-L plots indicates that the oxygen reduction reaction on all the three kinds of electrode surfaces is a well-defined first order reaction with respect to oxygen concentration. The calculated n_e are all close to 2 for all the three ligand systems, and the K-L curves are all parallel with the theoretical 2-electron curve (black dashed lines). The RDE results show that among the two kinds of ORR pathways, the 2-electron mechanism dominates on the ligand coordinated TMPPCo, yielding H_2O_2 as the final reduction product.

The kinetic current under the selected potentials (0.2 and 0.1 V) could be deduced from the y-axis intercept of K-L plot according to the K-L equation and is shown in Fig. 4a. Under each of the two selected potentials, the MPy system presents the largest kinetic current while MBN having the lowest. This means that the reaction kinetics of ORR on TMPPCo decreases in the order of: MPy > APT > MBN.

The mass transfer corrected Tafel plot is deduced using the ORR polarization curve collected under 150 r/min rotation and is depicted in Fig. 4b. The three polarization curves all exhibit similar Tafel slopes with values near 90 mV/dec. The similar Tafel slopes indicates the identical ORR mechanism for the three ligand coordinated TMPPCo complexes. Therefore, the deviation in onset potential should be due to different weakening abilities of the Co(II) center toward the O═O double bond which is induced by the axial

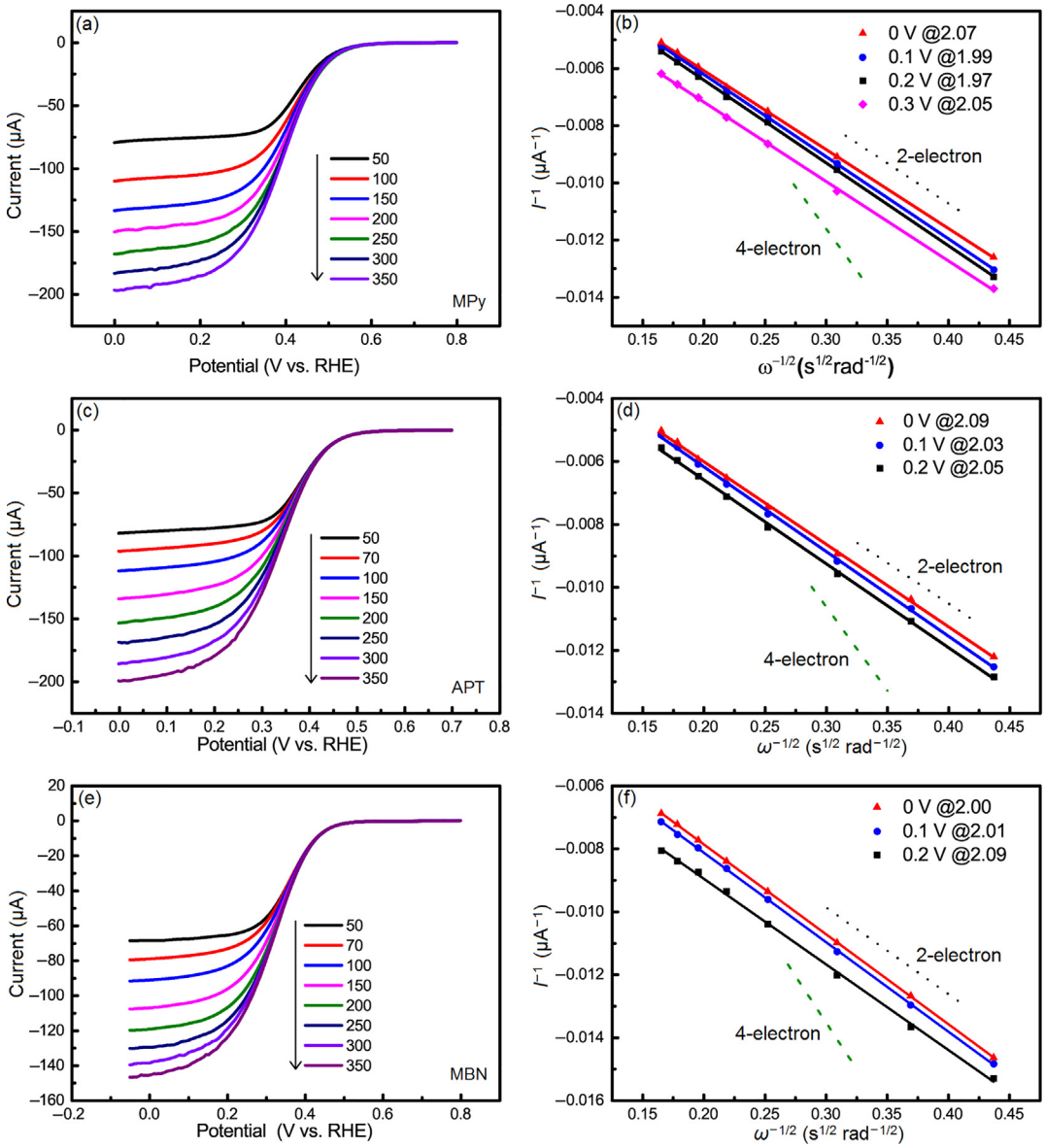

Fig. 3. (Color online) RDE voltammetric (a, c, e) and the corresponding K-L (b, d, f) curves of the gold disk electrodes modified with MPy, APT and MBN (from top to below) axially coordinated TMPPCo in ORR polarization region under different rotation speeds. The legends of the K-L curves denote the calculated electron transfer number under the corresponding potential. The black and green dashed lines in the right panels denote the theoretical 2-electron and 4-electron K-L curves, respectively.

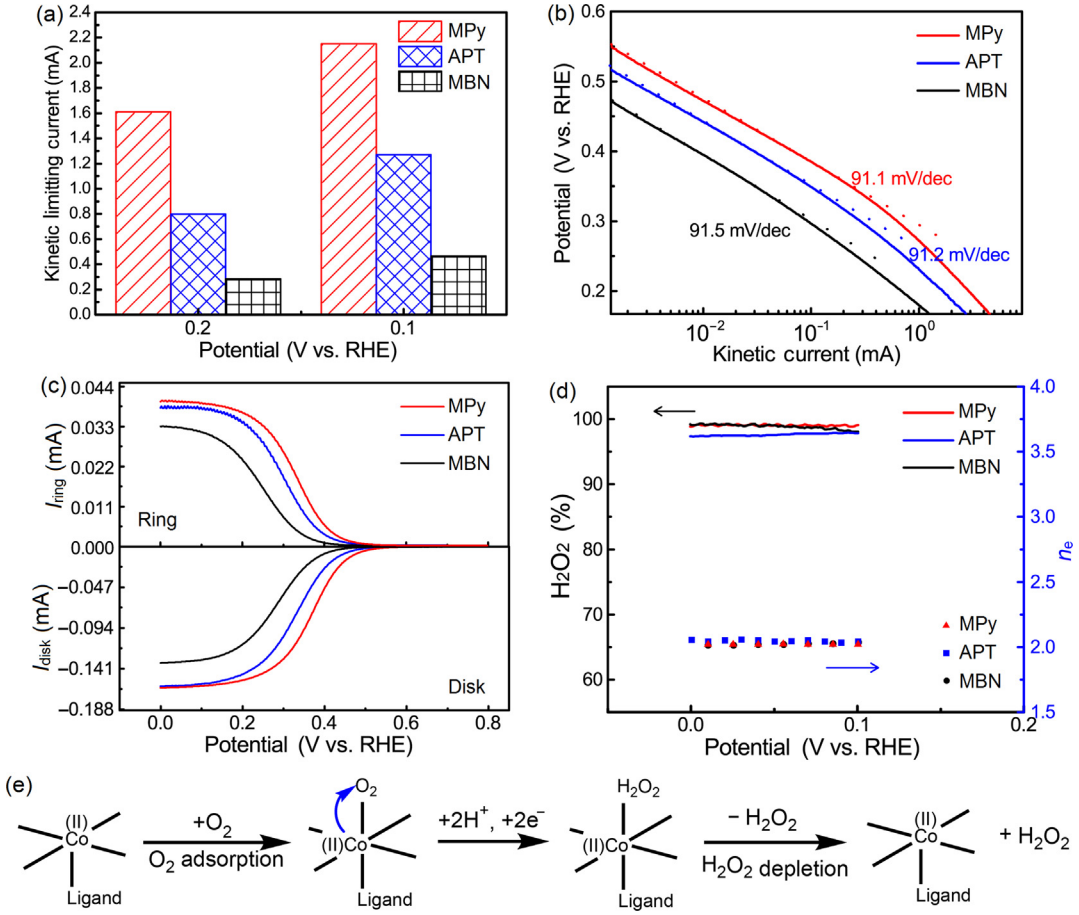

Fig. 4. (Color online) (a) Kinetic current values at 0.1 and 0.2 V. (b) Mass transfer corrected Tafel plot for the ORR polarization curves. (c) RRDE voltammetric curves under 150 rpm with the scan rate of 20 mV/s and a Pt ring potential of 1.2 V versus RHE. (d) H_2O_2% and n_e determined from RRDE data. (e) Schematic illustration on the 2-electron ORR mechanism on axially-coordinated TMPPCo.

ligand. The information revealed by the Tafel plot agrees well with the results of RDE tests. The axial ligand does not interfere with the ORR mechanism on ligand-coordinated TMPPCo, but possibly modifies the O═O weakening procedure through the electronic "push effect".

The rotating disk-ring electrode (RRDE) technique was employed to monitor the production of partial reduced oxygen species (PROS) during ORR, which is considered mainly as H_2O_2 in acidic medium. The Pt ring potential was held at 1.2 V (vs. RHE) to oxidize the H_2O_2 produced from the disk. The recorded disk and ring currents are shown in Fig. 4c. The H_2O_2 production yield (H_2O_2%) and apparent electron transfer number (n_e) could be determined using the following equations:

$$H_2O_2\% = 200 \times \frac{I_r}{N \times I_d + I_r}, \quad (1)$$

$$n_e = 4 \times \frac{I_d}{I_d + I_r/N}, \quad (2)$$

where I_d and I_r are the disk current and ring current, respectively; N is the collection efficiency of the RRDE setup which is measured to be 25% (Fig. S1 online). The calculated H_2O_2% and n_e values are shown in Fig. 4d. It is observed that the H_2O_2 production yield for the three ligand systems all exceed 95% with calculated n_e values close to 2, indicating that the ORR in the three systems all go through the 2-electron pathway with most of the reduction products being H_2O_2. This result matches well with that of RDE tests, further demonstrating that the 2-electron ORR mechanism of TMPPCo in acidic medium is not altered by the axial ligand.

Polarization curves with 1 mmol/L H_2O_2 in the ORR potential regime under N_2 atmosphere were recorded to check if H_2O_2 could be reduced on the axial vacancy of axially coordinated TMPPCo. No apparent Faradaic wave could be observed on the CVs (Fig. S5 online), which means that H_2O_2 cannot be reduced in this potential regime. This finding supports the results of RDE and RRDE tests, which demonstrates that the adsorbed O_2 on the axially-coordinated TMPPCo is only reduced to H_2O_2 and the further electro-reduction of H_2O_2 could not proceed, so the total electron transfer number in ORR is 2.

3.5. Computational results

To get further insights into the microscopic mechanism on the role of axial ligand in tuning the TMPPCo catalyzed ORR, first principles density function theory (DFT) based calculation is carried out. Fig. 4e depicts the possible 2-electron mechanism for O_2 reduction on ligand complexed TMPPCo.

It is generally accepted that the catalytic site of transition metal-based N_4-metallomacrocyclic molecules in electrocatalytic reactions is their metal center, on which the substrate molecule is adsorbed and subsequently activated through an inner-sphere interaction [7]. The oxygen reduction reaction initiates with the adsorption of oxygen molecules on the unoccupied axial vacancy of TMPPCo central cobalt ion. After forming the O_2-bounded adduct, the O═O double bond within the O_2 is weakened which

triggers the following reduction reaction. The back-bonding between the Co(II) center and O_2 molecule, which describes the partial electron injection from the *d* band of cobalt ion into the π^* orbital of adsorbed O_2, has been suggested to play a crucial role in determining the feasibility for both the O_2 adsorption process and the O═O double bond activation procedure [47,48]. Therefore, computational analysis on ligand-coordinated porphyrin is carried out to investigate the factors that might be altered by the axial ligand and then exert influence on the back-bonding procedure.

Fig. 5a depicts the fully optimized molecular structures of the uncoordinated porphyrin and ligand-coordinated cobalt porphyrins. The calculated atomic distances within the porphyrin ring ($R(Co\text{-}N_{Por})$) agrees well with previously reported values (Table S1 online), which demonstrates the validity of our calculations. Meanwhile, the atomic distance between the Co(II) center and ligand N atom ($R(Co\text{-}N_{Lig})$) is obviously smaller than the sum of their van der Waals radius [49] in all three ligand-coordinated porphyrin systems (Table 1), which indicates the strong chemical interaction between the cobalt porphyrin and the axial ligand.

The atomic charge of porphyrin central ion is one of the several important factors that might affect the back-bonding formation and a higher positive charge of the metal center would lead to weaker back-donation and less stable adsorption while a smaller positive charge could enhance the back-bonding formation and trigger the more stable bonding of the adsorbate [47]. The Hirshfeld atomic charge (Q_{Co}) distributed on the central cobalt(II) ion in the optimized configuration is analyzed (Fig. 5a). As shown in Table 1, the positive charge accumulated on cobalt ion without the axial ligand is 0.263e. The introduction of three different axial ligands leads to different extents of decrease in the charge population of the central cobalt(II) ion, which is due to the electron donation effect from the axial ligand (donor) toward the cobalt ion (acceptor). An increasing order in positive charge population of cobalt(II) ion when porphyrin is complexed with axial ligands is presented as follows: MPy < APT < MBN. Since the MPy system is least positively charged on Co(II) center, the back electron-donation from cobalt ion toward the π^* orbital of O_2 is most efficient, which promotes the adsorption and activation of O_2 on the reaction site. For APT and MBN systems, the positive charge population of cobalt ion is slightly larger, which is not favored for the back-bonding formation between cobalt ion and O_2, so the catalytic reduction of O_2 should be harder in these two systems as compared with the MPy system.

The energy level of the frontier molecular orbitals, including highest singly occupied molecular orbital (SOMO) and lowest unoccupied molecular orbital (LUMO), of cobalt porphyrin has a great impact on the back-bonding process and a higher HOMO energy could facilitate the partial *d* electron transfer process from the metal ion toward the π^* orbital of O_2, producing stronger weakening toward the O═O double bond [48]. As is shown in Fig. 5b, the interaction with three axial ligands all leads to the increase in SOMO level of cobalt porphyrin, which indicates the promoted back-bonding for O_2 adsorbate compared with the case of uncoordinated cobalt porphyrin.

Although the above-mentioned computational results could not be directly correlated to the observed difference in ORR onset potential, a microscopic understanding toward the internal effects of axial ligand in tuning the ORR activity of cobalt porphyrin has

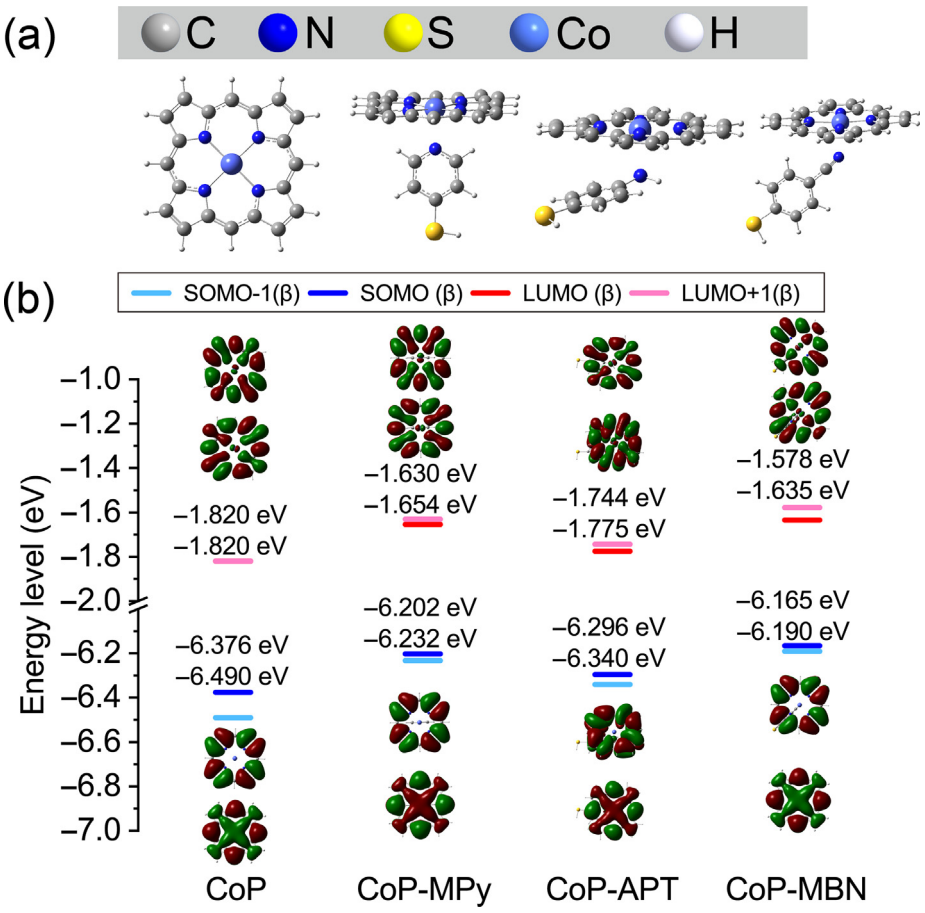

Fig. 5. (a) Optimized structures of uncoordinated cobalt porphyrin and MPy, APT, MBN complexed cobalt porphyrins. (b) Electron density distribution and energy profiles of frontier molecular orbitals in cobalt porphyrin and axial ligand coordinated porphyrins, obtained from DFT calculation.

Table 1
Calculated properties of the optimized cobalt porphyrin (CoP) and ligand coordinated porphyrins.

System	Spin multiplicity	Q_{Co} (e)	R(Co-N_{Por}) (Å)	R(Co-N_{Lig}) (Å)
CoP	2	+0.263	2.00	–
CoP-MPy	2	+0.171	2.02	2.24
CoP-APT	2	+0.182	2.02	2.33
CoP-MBN	2	+0.188	2.01	2.35

been realized. The participation of axial ligands modifies the charge density of central cobalt ion and also changes the frontier molecular orbital distribution within the porphyrin, both properties have influence on the back-bonding formation between the cobalt ion and O_2 adsorbate. Thus, the O_2 adsorption and the subsequent O═O weakening processes on the central cobalt ion are tailored and therefore affects the overall ORR activity. The ligand with a stronger binding ability such as MPy in this study leads to the more easily formed back-bonding, thus the ORR activity of the ligand coordinated cobalt porphyrin is higher. On the contrary, the back-bonding is weaker when a weak-binding ligand is involved which leads to a lower ORR activity of the porphyrin. More detailed DFT-based calculation on oxygen adsorption energy, Gibbs energy changes in elementary steps, and theoretical prediction on ORR onset potential is undergoing in our lab.

4. Conclusion

In summary, the "push effect" of axial ligand toward the catalytic activity of cobalt porphyrin has been studied using a model system. Three aromatic thiol ligands, MPy with pyridinic N atom, APT with —NH_2 and MBN with —CN as the ligand groups have been adopted to impose different extends of electronic donating effect on the Co(II) center of the TMPPCo model molecule. The titled SAM formation of these thiol ligands on Au electrode surface has been confirmed by Raman and electrochemical characterizations, which is necessary for the construction of the desired molecular structure on electrode surface. The catalytic activity of the TMPPCo monolayers on ligand SAM coated Au electrode toward ORR in 0.5 mol/L H_2SO_4 is compared among the three ligands, which exhibits a maximum onset potential difference of 80 mV between the MPy and the MBN systems. The ORR activity of ligand-complexed cobalt porphyrin increases with the increase in coordination strength of the axial ligands. The mechanism study with RDE and RRDE techniques declares no difference in the 2-electron ORR pathway for all the three ligand coordinated TMPPCo systems. The H_2O_2 polarization study has evidenced the inability in H_2O_2 decomposition for ligand complexed porphyrin. The origins for the difference in ORR activity are explored using theoretical calculation, which unravels the modification of positive charge on central cobalt ion and altered frontier molecular orbital distribution on TMPPCo by the axial ligand. Both properties have severe impact on the back-bonding formation between Co(II) center and adsorbed O_2, which might affect the important elemental steps in ORR, including oxygen adsorption and O═O double bond weakening procedure. Through this way, the overall ORR activity of cobalt porphyrin can be efficiently tailored by the engineering of using different axial ligands.

Conflict of interest

The authors declare that they have no conflict of interest.

Acknowledgments

This work was supported by the National Key Research and Development Program of China (2017YFA0206500), and the National Natural Science Foundation of China (21635004, 21675079).

Author contributions

Yue Zhou, Feng-Bin Wang and Xing-Hua Xia designed experiments. Yue Zhou and Yong-Fang Xing carried out the experiments. Jing Wen and Haibo Ma performed the DFT calculation. Yue Zhou, Haibo Ma and Xing-Hua Xia wrote the manuscript.

Appendix A. Supplementary data

Supplementary data to this article can be found online at https://doi.org/10.1016/j.scib.2019.07.003.

References

[1] Jasinski R. A new fuel cell cathode catalyst. Nature 1964;201:1212.
[2] Lei H-T, Liu C-Y, Wang Z-J, et al. Noncovalent immobilization of a pyrene-modified cobalt corrole on carbon supports for enhanced electrocatalytic oxygen reduction and oxygen evolution in aqueous solutions. ACS Catal 2016;6:6429–37.
[3] Zagal JH, Koper MT. Reactivity descriptors for the activity of molecular MN_4 catalysts for the oxygen reduction reaction. Angew Chem Int Ed 2016;55:14510–21.
[4] Levy N, Mahammed A, Kosa M, et al. Metallocorroles as nonprecious-metal catalysts for oxygen reduction. Angew Chem Int Ed 2015;54:14080–4.
[5] Zhang W, Lai W-Z, Cao R. Energy-related small molecule activation reactions: oxygen reduction and hydrogen and oxygen evolution reactions catalyzed by porphyrin- and corrole-based systems. Chem Rev 2017;117:3717–97.
[6] Ou Z-P, Lu A-X, Meng D-Y, et al. Molecular oxygen reduction electrocatalyzed by *meso*-substituted cobalt corroles coated on edge-plane pyrolytic graphite electrodes in acidic media. Inorg Chem 2012;51:8890–6.
[7] Masa J, Ozoemena K, Schuhmann W, et al. Oxygen reduction reaction using N_4-metallomacrocyclic catalysts: fundamentals on rational catalyst design. J Porphyr Phthalocya 2012;16:761–84.
[8] Zagal JH. Metallophthalocyanines as catalysts in electrochemical reactions. Coord Chem Rev 1992;119:89–136.
[9] Banham D, Ye S-Y, Pei K, et al. A review of the stability and durability of non-precious metal catalysts for the oxygen reduction reaction in proton exchange membrane fuel cells. J Power Sources 2015;285:334–48.
[10] Baranton S, Coutanceau C, Roux C, et al. Oxygen reduction reaction in acid medium at iron phthalocyanine dispersed on high surface area carbon substrate: tolerance to methanol, stability and kinetics. J Electroanal Chem 2005;577:223–34.
[11] Liu B-C, Brückner C, Lei Y, et al. Cobalt porphyrin-based material as methanol tolerant cathode in single chamber microbial fuel cells (SCMFCs). J Power Sources 2014;257:246–53.
[12] Zagal J, Paez M, Tanaka A, et al. Electrocatalytic activity of metal phthalocyanines for oxygen reduction. J Electroanal Chem 1992;339:13–30.
[13] Osmieri L, Monteverde Videla AH, Ocón P, et al. Kinetics of oxygen electroreduction on Me–N–C (Me= Fe Co, Cu) catalysts in acidic medium: insights on the effect of the transition metal. J Phys Chem C 2017;121:17796–817.
[14] Yuasa M, Nishihara R, Shi C, et al. A comparison of several meso-tetraalkyl cobalt porphyrins as catalysts for the electroreduction of dioxygen. Polym Adv Technol 2001;12:266–70.
[15] Zagal JH, Gulppi M, Isaacs M, et al. Linear versus volcano correlations between electrocatalytic activity and redox and electronic properties of metallophthalocyanines. Electrochim Acta 1998;44:1349–57.
[16] Wang J, Wang TT, Zhang DY, et al. Exploration of the copper active sites in electrooxidation of glucose on a copper/nitrogen doped graphene nanocomposite. J Phys Chem C 2016;120:15593–9.
[17] Karlin KD. Bioinorganic chemistry: model offers intermediate insight. Nature 2010;463:168–9.
[18] Wang J, Wang K, Wang F, et al. Bioinspired Cu catalyst effective for both reduction and evolution of oxygen. Nat Commun 2014;5:5285.
[19] Wang J, Lin W, Shi Y, et al. A simple way to fine tune the redox potentials of cobalt ions encapsulated in nitrogen doped graphene molecular catalysts for oxygen evolution reaction. Chem Commun 2016;52:13409–12.
[20] Murgida DH, Hildebrandt P. Redox and redox-coupled processes of heme proteins and enzymes at electrochemical interfaces. Phys Chem Chem Phys 2005;7:3773–84.

[21] Cao R-G, Thapa R, Kim H, et al. Promotion of oxygen reduction by a bio-inspired tethered iron phthalocyanine carbon nanotube-based catalyst. Nat Commun 2013;4:2076.
[22] Wang G-X, Zhou Y, Wang M, et al. Structure orientation of hemin self-assembly layer determining the direct electron transfer reaction. Chem Commun 2015;51:689–92.
[23] He F, Mi L, Shen Y-F, et al. Driving electrochemical oxygen reduction and hydrazine oxidation reaction by enzyme-inspired polymeric Cu(3,3′-diaminobenzidine) catalyst. J Mater Chem A 2017;5:17413–20.
[24] Samanta S, Das PK, Chatterjee S, et al. Effect of axial ligands on electronic structure and O_2 reduction by iron porphyrin complexes: towards a quantitative understanding of the "push effect". J Porphyr Phthalocya 2015;19:92–108.
[25] Christoforidis KC, Pantazis DA, Bonilla LL, et al. Axial ligand effect on the catalytic activity of biomimetic Fe-porphyrin catalyst: an experimental and DFT study. J Catal 2016;344:768–77.
[26] Silva JF, Pavez J, Silva CP, et al. Electrocatalytic activity of modified gold electrodes based on self-assembled monolayers of 4-mercaptopyridine and 4-aminothiolphenol on Au (111) surfaces chemically functionalized with substituted and unsubstituted iron phthalocyanines. Electrochim Acta 2013;114:7–13.
[27] Meunier B, de Visser SP, Shaik S. Mechanism of oxidation reactions catalyzed by cytochrome P450 enzymes. Chem Rev 2004;104:3947–80.
[28] Green MT. Role of the axial ligand in determining the spin state of resting cytochrome P450. J Am Chem Soc 1998;120:10772–3.
[29] Rittle J, Green MT. Cytochrome P450 compound I: capture, characterization, and C-H bond activation kinetics. Science 2010;330:933–7.
[30] Cheng Q-Q, Yang L-J, Zou L-L, et al. Single cobalt atom and N codoped carbon nanofibers as highly durable electrocatalyst for oxygen reduction reaction. ACS Catal 2017;7:6864–71.
[31] Kudelski A, Bukowska J. Charge-transfer contribution to surface-enhanced Raman scattering and surface-enhanced resonance Raman scattering of dyes at silver and gold electrodes. Chem Phys Lett 1996;253:246–50.
[32] Frisch M-J, Trucks G-W, Schlegel H-B, et al. Gaussian 09, Revision D. 01. Wallingford CT: Gaussian, Inc.; 2009.
[33] Li YR, Wen J, Qin M, et al. Single-molecule mechanics of catechol-iron coordination bonds. ACS Biomater Sci Eng 2017;3:979–89.
[34] Moskovits M, Suh J. Surface selection rules for surface-enhanced Raman spectroscopy: calculations and application to the surface-enhanced Raman spectrum of phthalazine on silver. J Phys Chem 1984;88:5526–30.
[35] Holze R. Competition of anchoring groups in adsorption on gold electrodes—a comparative spectroelectrochemical study of 4-mercaptobenzonitrile and aromatic nitriles. J Solid State Electrochem 2013;17:1869–79.
[36] Liu H-L, Cao J, Hanif S, et al. Size-controllable gold nanopores with high SERS activity. Anal Chem 2017;89:10407–13.
[37] Kim K, Shin D, Choi J-Y, et al. Surface-enhanced Raman scattering characteristics of 4-aminobenzenethiol derivatives adsorbed on silver. J Phys Chem C 2011;115:24960–6.
[38] Kim K, Yoon JK. Raman scattering of 4-aminobenzenethiol sandwiched between Ag/Au nanoparticle and macroscopically smooth Au substrate. J Phys Chem B 2005;109:20731–6.
[39] Hu J-W, Zhao B, Xu W-Q, et al. Surface-enhanced Raman spectroscopy study on the structure changes of 4-mercaptopyridine adsorbed on silver substrates and silver colloids. Spectrochim Acta A 2002;58:2827–34.
[40] Guo H, Ding L, Mo Y-J. Adsorption of 4-mercaptopyridine onto laser-ablated gold, silver and copper oxide films: a comparative surface-enhanced Raman scattering investigation. J Mol Struct 2011;991:103–7.
[41] Kemnade N, Chen Y, Muglali MI, et al. Electrochemical reductive desorption of alkyl self-assembled monolayers studied in situ by spectroscopic ellipsometry: evidence for formation of a low refractive index region after desorption. Phys Chem Chem Phys 2014;16:17081–90.
[42] Kang H, Noh J. Influence of thiol molecular backbone structure on the formation and reductive desorption of self-assembled aromatic and alicyclic thiol monolayers on Au(111) surface. Bull Korean Chem Soc 2013;34:1383–7.
[43] Sato Y, Mizutani F. Formation and characterization of aromatic selenol and thiol monolayers on gold: in-situ IR studies and electrochemical measurements. Phys Chem Chem Phys 2004;6:1328–31.
[44] Jin Q, Rodriguez J, Li C-Z, et al. Self-assembly of aromatic thiols on Au (111). Surf Sci 1999;425:101–11.
[45] Wang Q, Zhi F-P, Wang W-T, et al. Direct electron transfer of thiol-derivatized tetraphenylporphyrin assembled on gold electrodes in an aqueous solution. J Phys Chem C 2009;113:9359–67.
[46] Liu H-S, Zhang L, Zhang J-J, et al. Electrocatalytic reduction of O_2 and H_2O_2 by adsorbed cobalt tetramethoxyphenyl porphyrin and its application for fuel cell cathodes. J Power Sources 2006;161:743–52.
[47] Khade RL, Yang Y-W, Shi Y-L, et al. HNO-binding in heme proteins: effects of iron oxidation state, axial ligand, and protein environment. Angew Chem Int Ed 2016;55:15058–61.
[48] Sun S-R, Jiang N, Xia D-G. Density functional theory study of the oxygen reduction reaction on metalloporphyrins and metallophthalocyanines. J Phys Chem C 2011;115:9511–7.
[49] Batsanov SS. Van der Waals radii of elements. Inorg Mater 2001;37:871–85.

Yue Zhou received his B.S. degree from Nanjing Normal University. He is now a Ph.D. candidate in Nanjing University under the guidance of Prof. Xing-Hua Xia. His research focuses on the electrocatalytic and photo-electrochemical properties of oriented molecular assembly on surfaces and interfaces.

Hai-Bo Ma is a Professor at School of Chemistry and Chemical Engineering, Nanjing University. His research interests include: (1) density matrix renormalization group and other advances on numerical renormalization group methods for large correlated systems; (2) molecule design through Materials Genome Initiative by via machine learning and high-throughput computational virtual screening; (3) optoelectronic processes in organic photovoltaics; (4) excited states in macromolecules and condensed phases.

Feng-Bin Wang received her B.S. degree from Shandong University in 1998, and Ph.D. degree from Changchun Institute of Applied Chemistry, Chinese Academy of Sciences in 2003. She now works as a teacher at School of Chemistry and Chemical Engineering, Nanjing University. Her research interests include: (1) fabrication of nanomaterials for the application in biosensing and fuel cells; (2) micro/nanofluidic bioanalytical systems.

Xing-Hua Xia is a Professor at the State Key Laboratory of Analytical Chemistry in Nanjing University. The ongoing researches in Xia's group include: (1) the understanding of bio- and chemical processes occurring at interfaces/surfaces: kinetics and mechanism of bio/electro-chemical catalysis reactions at functional electrode surfaces using in situ spectroscopic techniques, relationship between conformation and orientation of biomolecules and their functions of direct electron transfer and biocatalytic activity; (2) mass transport in micro/nanofluidic systems; (3) synthesis of bio-inspired functional materials for electrochemical energy conversion and storage.